Polarizability and hyperpolarizability of BN zigzag nanotubes calculated by the coupled perturbed Kohn-Sham scheme

Matteo Ferrabone,[1] Bernard Kirtman,[2] Michel Rérat,[3] Roberto Orlando,[4] and Roberto Dovesi[1]

[1]*Dipartimento di Chimica IFM, Università di Torino and NIS (Nanostructured Interfaces and Surfaces), Centre of Excellence, Via P. Giuria 7, IT-10125 Torino, Italy*

[2]*Department of Chemistry and Biochemistry, University of California, Santa Barbara, California 93106, USA*

[3]*Equipe de Chimie Physique, IPREM UMR5254, Université de Pau et des Pays de l'Adour, FR-64000 Pau, France*

[4]*Dipartimento di Scienze e Tecnologie Avanzate, Università del Piemonte Orientale, Viale T. Michel 11, IT-15121 Alessandria, Italy*

(Received 12 November 2010; revised manuscript received 5 May 2011; published 16 June 2011)

Linear and nonlinear electric dipole susceptibilities are evaluated for infinite periodic zigzag BN nanotubes utilizing primarily the coupled perturbed Kohn-Sham scheme recently implemented in the CRYSTAL code. The effect of different functionals, basis set, and computational parameters is examined. Most of the calculations are done at the B3LYP/6-31G* level. For electronic linear polarizabilities, substantial differences compared to the uncoupled sum-over-states scheme are found. Much larger radii were considered than in earlier studies, thereby permitting accurate comparison with corresponding properties of the hexagonal monolayer. In addition, we confirmed the dielectric shell model for the linear polarizability, but with a significantly different shell thickness than previously thought. Vibrational (ionic) contributions to the nonlinear susceptibilities are calculated. In doing so, the finite-field–nuclear-relaxation (FF–NR) method was employed for the transverse components of the (6,0), (9,0), and (12,0) nanotubes. Aside from being computationally more efficient than other procedures, this method includes anharmonicity effects through first order and, as shown, is readily applied to key dynamic as well as static properties (and yields the static linear polarizability as well). Our calculated nonlinear vibrational susceptibilities sometimes exceed, or even greatly exceed, the corresponding static electronic susceptibility. In such cases, the relative magnitude of the vibrational contribution grows substantially with tube radius over the range considered. Future plans include extending these FF–NR calculations to large nanotubes and to the longitudinal (periodic) direction as well.

DOI: 10.1103/PhysRevB.83.235421 PACS number(s): 73.22.−f, 71.10.−w, 71.15.−m

I. INTRODUCTION

Since their discovery,[1] carbon nanotubes (CNTs) have attracted the attention of the scientific community for their unique electrical, mechanical, and thermal properties.[2] Almost immediately thereafter there began a search for noncarbon nanotubes. Based on the analogy between graphite and hexagonal boron nitride (h-BN), the existence of BN nanotubes (BNNTs) was proposed theoretically[3,4] in 1994 and found experimentally the next year.[5] Although h-BN and graphite are isoelectronic, and have very similar structures, the corresponding nanotubes show significant differences in their properties. In particular, BNNTs have greater thermal stability[6] and, thanks to a wide band gap ($\simeq$ 5.5 eV), a less dramatic dependence of the electrical properties on rolling direction and tube radius. The stability of the properties with respect to tube size is an important advantage of BNNTs over CNTs. For the latter, poor control of tube chirality and tube size leads to poor control of tube properties. As a result, BNNTs have been the object of extensive experimental[7–13] and theoretical[14–18] studies because of their possible applications in such fields as super-tough composite materials and nanoelectronic devices.

A single-walled BN nanotube (SWBNNT) is formed by rolling an h-BN monolayer into a cylinder along an (n_1,n_2) lattice vector. The n_1 and n_2 indices determine the radius and chirality, which are the key parameters that characterize the structure.[19,20] Multiwalled nanotubes can be obtained with two or more SWBNNTs of different radii but the same axes. Despite a flurry of theoretical investigations on SWBNNTs in recent years[14–17,21] (all dealing with tubes of radius smaller than 15 Å), there remain a number of open, or not fully resolved, issues concerning their electric field response. The most recent treatments of the polarizability of BNNTs (Refs. 16, 17, and 21) were carried out using density functional theory (DFT) with either the local density approximation (LDA) or generalized gradient approximation[17] (GGA) and supercell geometry. These calculations employ a plane-wave basis (or projector-augmented plane waves) and do not include exact exchange. To our knowledge, only the linear polarizability (referred to hereafter simply as polarizability) has been considered thus far. In view of the well-known overshoot of polarizabilities obtained for LDA and GGA functionals in quasi-1D systems,[22–26] a comparison with Hartree-Fock (HF) and, particularly, with the hybrid B3LYP functional is of interest. These aspects are studied here using the CRYSTAL code, which employs a local Gaussian atomic orbital basis, and has the capability for carrying coupled perturbed HF and Kohn-Sham (CPHF and CPKS) calculations.

It is known from LDA calculations by Guo *et al.*[16] that there is a substantial vibrational (sometimes called ionic) contribution to the static polarizability of BNNTs. Their results were obtained by finite differences using finite-field electric-enthalpy theory for nanotubes of radius up to 15 Å. Aside from this treatment, we utilize an alternative computational procedure known as the finite-field–nuclear-relaxation (FF–NR) method.[27] The latter also yields, with little extra effort,

the static vibrational hyperpolarizabilities as well as the vibrational contribution to most key dynamic nonlinear optical processes. This method, unlike the treatment employed by Guo *et al.*, does not require explicit evaluation of vibrational force constants but, nonetheless, accounts for effects due to vibrational and electrical anharmonicity, at least through the first order of perturbation theory. Morevoer, there is an advanced version (not utilized here) that, in principle, gives a complete accounting of anharmonicity contributions.[28] The FF–NR method has been used previously for ordinary small to medium size molecules, but this is the first application to a nanotube or any other periodic system. Although currently implemented in the CRYSTAL program only for nonperiodic nanotube directions, a formulation for periodic directions is available[29] and is currently being added to the code. Finally, in order to separate the electronic and vibrational contributions, static electronic hyperpolarizabilities are required. For the representative (6,0), (9,0), and (12,0) zigzag nanotubes considered in this initial application, they are obtained by the analytical CPKS (Refs. 30–32) procedure, as well as the FF method, in order to provide a check on both.

There has been much discussion in the literature concerning the linear versus quadratic behavior of the transverse component of the nanotube polarizability (per unit length) as a function of the tube radius. It originates with a paper by Benedict *et al.*,[33] who developed a treatment for single-walled carbon tubes based on a thin conducting cylindrical shell model that leads to a quadratic dependence. Very recently, Lan *et al.*[17] have proposed a more appropriate model for SWBNNTs wherein the conducting shell is replaced by a dielectric shell with uniform dielectric constant. Their model reproduces the linear dependence on radius found in earlier LDA calculations.[14,21,34] Here, we test the adequacy of this form using our own B3LYP calculations for nanotubes with radii up to 24 Å. The extension to much larger radii than previously considered turns out to be essential for obtaining an accurate extrapolation to the monolayer limit, which further confirms the numerical accuracy of our method.

The computational techniques employed to determine the electronic and vibrational (hyper)polarizabilities are given in the next section. As far as the electronic properties are concerned, the CPHF and CPKS implementations in CRYSTAL have been described elsewhere.[30,35–38] Thus, we focus here on the parameters that control the accuracy of the self-consistent field (SCF) treatment and the geometry optimization, along with the choice of basis set. A brief review of the Berry phase treatment of the static vibrational polarizability is presented along with a fuller exposition of the FF–NR method. The latter is applicable as well to static and dynamic vibrational hyperpolarizabilities. Although the FF–NR method is well known to quantum chemists, additional details are provided for the materials physics community. Our results are reported and discussed in Sec. III. Aspects covered include geometry, band gap, effect of orbital relaxation and exact exchange on the polarizability, dependence of the transverse polarizability on the tube radius, and FF–NR transverse vibrational (hyper)polarizabilities. The concluding section contains a summary of our major findings together with some plans for future work.

II. COMPUTATIONAL METHODS AND DETAILS

Our CPHF and CPKS calculations of electronic (hyper)polarizabilities were performed with a development version[37] of the periodic *ab initio* CRYSTAL09 code.[39] The CPKS procedure is a (linear and quadratic) response formulation of time-dependent DFT. Thus, in principle, it includes all contributions to the (hyper)polarizability such as excitonic effects. In practice, our results are subject to the limitations of the hybrid B3LYP functional that is used here.

DFT exchange-correlation contributions were evaluated by numerical integration over the unit-cell volume. Radial and angular points of the integration grid are generated through Gauss-Legendre radial quadrature and Lebedev two-dimensional angular point distributions. In our calculations, a (75 974) pruned grid (XLGRID keyword in the CRYSTAL09 manual),[40] corresponding to 75 radial and 974 angular points, was employed. The integration accuracy can be estimated by the error in the electronic charge per unit cell $\Delta_e = 2.8 \times 10^{-3}|e|$ [out of a total of 288 electrons for the (12,0) BNNT], obtained by using a 6-31G* basis set with the exponent of the most diffuse valence shell energy optimized at the equilibrium geometry. Other details on the grid generation and its influence on the accuracy and cost can be found in Refs. 41–43.

Evaluation of the Coulomb and exact exchange infinite series is controlled by five parameters[40] (T_1, T_2, T_3, T_4, T_5), the values of which are set to $T_1 = T_2 = T_3 = T_4 = \frac{1}{2}T_5 = T_I$. The effect of T_I and S, the shrinking factor used to generate the commensurate net of points at which the Fock and KS matrix is diagonalized and the CPHF and CPKS equations are solved, is shown in Table I for the same (12,0) tube, basis set and geometry as above. It turns out that a very rapid convergence with increasing value of these two parameters is achieved. In this paper, $T_I = 8$ and $S = 16$ are used.

Convergence of the SCF zeroth-order energy and CPHF and CPKS iterations is controlled by the T_E and T_{CP} parameters, respectively. The SCF cycles are terminated when the difference Δ between the values of the total energy (E, in Hartree) or polarizability (α, in Bohr^3), for two successive cycles, is less than 10^{-T_E} or $10^{-T_{CP}}$, respectively. In this paper, $T_E = 10$ and $T_{CP} = 4$ and 1 for the first- and second-order CPHF and CPKS cycles, respectively. Sometimes, the iterations produced large oscillations of the Fock and KS matrices, in which case these matrices were damped by mixing at the m and $m - 1$ cycles

TABLE I. Effect of the shrinking factor (S) and of the tolerance parameter for truncation of the Coulomb and exchange series (T_I) on the (12,0) BN nanotube electronic polarizability tensor (in Å^3 and per BN unit). Calculations performed at the equilibrium geometry with B3LYP/6-31G*. $S = 16$ and $T_I = 8$ are used when not specified.

		$\alpha^{\parallel}$		$\alpha^{\perp}$	
		SOS	CPKS	SOS	CPKS
S	4	4.108	4.712	2.952	1.680
	8	4.049	4.644	2.952	1.680
	16	4.048	4.644	2.952	1.680
T_I	7	4.050	4.645	2.953	1.680
	8	4.048	4.644	2.952	1.680
	9	4.049	4.644	2.952	1.680

TABLE II. Effect of basis set on the (12,0) BN nanotube properties. ΔE (in μHa) is the energy difference with respect to the richest basis set [6-31G**(f)], BG is the band gap (in eV), and the electronic polarizabilities are in Å^3 per BN unit. $S = 16$, $T_I = 8$, and B3LYP are used. All calculations performed at the equilibrium geometry determined for each basis set. The values in parentheses are the percentage differences with respect to the richest basis.

			$\alpha^{\parallel}$		$\alpha^{\perp}$	
Basis	ΔE	BG	SOS	CPKS	SOS	CPKS
6-31G	643.6	5.98	3.922 (−5)	4.571 (−4)	2.718 (−11)	1.653 (−3)
6-31G*	136.1	5.94	4.048 (−2)	4.645 (−2)	2.952 (−3)	1.680 (−1)
6-1111G*	13.6	5.93	4.046 (−2)	4.634 (−2)	2.978 (−2)	1.684 (−1)
6-31G**	89.2	5.93	4.091 (−1)	4.698 (−1)	2.996 (−1)	1.691 (−1)
6-31G**(f)		5.94	4.133	4.743	3.038	1.706

with the FMIXING parameter[40] of 30% and 50% for the SCF and CPHF and CPKS calculations, respectively.

The sufficiency of the 6-31G* basis set for determination of total energy, band gap (BG), and polarizability was explored as documented in Table II. Polarizabilities differ by less than 2% from those obtained with much richer basis sets; for this reason, the 6-31G* basis was used for subsequent steps of this study.

The dependence of the (12,0) electronic polarizability on the DFT functional (again, for the same basis set and geometry as above) is shown in Table III. The uncoupled sum-over-states (SOS) values are also reported in the table in order to see the influence of orbital relaxation. These results will be discussed in the next section.

The fractional atomic coordinates and unit-cell parameters[44–46] were optimized within a quasi-Newton scheme using analytical energy gradients combined with the Broyden-Fletcher-Goldfarb-Shanno algorithm for Hessian updating.[47–50] Convergence was checked on gradient components and nuclear displacements. For both, a threshold of 0.000 03 a.u. was chosen.

For the complete set of nanotubes considered in this study, the total static polarizability was determined from

$$\alpha^0 = \alpha^e + \sum_j \frac{\overline{Z}_j^2}{\nu_j^2}, \tag{1}$$

where α^e is the electronic (clamped ion) contribution. The vibrational (ionic) contribution is given, in the double harmonic approximation, by the second term on the right-hand side. In this term, $\overline{Z}_j^2$ is a mass weighted effective mode Born charge and ν_j is a vibrational frequency. Born charges were calculated using a Berry phaselike scheme,[51,52] while frequencies were obtained by diagonalizing the dynamical matrix, found by numerical differentiation of the analytical energy gradients (see Ref. 41 for details).

For the (6,0), (9,0), and (12,0) nanotubes, the total static polarizability in the transverse direction was also evaluated by means of the FF–NR method.[27,28] The FF–NR computational scheme for static (hyper)polarizabilities can be summarized as follows.[27] If we denote the equilibrium geometry in a static electric field ($\mathbf{F}$) by $\mathbf{R_F}$ and without the field by $\mathbf{R_0}$, then a Taylor series expansion for the field-dependent dipole moment at the two geometries yields

$$\begin{aligned}(\Delta\mu_t)_{\mathbf{R_0}} &= \mu_t(\mathbf{F},\mathbf{R_0}) - \mu_t(\mathbf{0},\mathbf{R_0}) \\ &= \sum_u \alpha^e_{tu} F_u + \frac{1}{2}\sum_{u,v} \beta^e_{tuv} F_u F_v \\ &\quad + \frac{1}{6}\sum_{u,v,w} \gamma^e_{tuvw} F_u F_v F_w + \cdots \end{aligned} \tag{2}$$

and

$$\begin{aligned}(\Delta\mu_t)_{\mathbf{R_F}} &= \mu_t(\mathbf{F},\mathbf{R_F}) - \mu_t(\mathbf{0},\mathbf{R_0}) \\ &= \sum_u a^{\mu}_{tu} F_u + \frac{1}{2}\sum_{u,v} b^{\mu}_{tuv} F_u F_v \\ &\quad + \frac{1}{6}\sum_{u,v,w} g^{\mu}_{tuvw} F_u F_v F_w + \cdots . \end{aligned} \tag{3}$$

In Eq. (2), the superscript "e" refers to the clamped ion electronic value (evaluated at the equilibrium geometry). This value can be separately obtained experimentally as well as theoretically. Experimentally, one may carry out a nonresonant

TABLE III. Effect of the Hamiltonian on the (12,0) BN nanotube electronic polarizability tensor. Computational details and units are as in captions to previous tables.

		$\alpha^{\parallel}$		$\alpha^{\perp}$	
	BG	SOS	CPKS	SOS	CPKS
LDA	4.16	5.505	5.313	3.766	1.761
PBE	4.21	5.490	5.355	3.763	1.787
B3LYP	5.94	4.048	4.644	2.952	1.680
PBE0	6.36	3.798	4.492	2.788	1.652
HF	13.20	1.927	3.322	1.555	1.405

measurement at sufficiently high frequency that the vibrational contribution to the (hyper)polarizability is negligible. Then, in order to obtain the static value in Eq. (2) [and Eqs. (4)–(6) below], the nonresonant measurement must be extrapolated to zero frequency. The coefficients a^{μ}, b^{μ}, and g^{μ} give the static electronic plus vibrational (hyper)polarizability in the nuclear relaxation (NR) approximation (see, again, Ref. 27):

$$a^{\mu}_{tu} = \alpha^{e}_{tu}(0;0) + \alpha^{\mathrm{NR}}_{tu}(0;0), \tag{4}$$

$$b^{\mu}_{tuv} = \beta^{e}_{tuv}(0;0,0) + \beta^{\mathrm{NR}}_{tuv}(0;0,0), \tag{5}$$

$$g^{\mu}_{tuvw} = \gamma^{e}_{tuvw}(0;0,0,0) + \gamma^{\mathrm{NR}}_{tuvw}(0;0,0,0). \tag{6}$$

By comparison with the Bishop and Kirtman perturbation treatment,[53] the nuclear-relaxation term on the right-hand side of Eq. (4) is the double harmonic value of the vibrational polarizability. In principle, Eqs. (1) and (4) should give identical results. On the other hand, the static hyperpolarizabilities in Eqs. (5) and (6) also contain the first-order perturbation contributions due to anharmonic force constants and anharmonic electrical property derivatives (the first-order vibrational contribution to alpha vanishes and γ^{NR} contains, in addition, a second-order term). It is important to note that the anharmonic parameters are never explicitly evaluated. Similar expansions may be carried out for α^{e}:

$$\begin{aligned}\left(\Delta\alpha^{e}_{tu}\right)_{\mathbf{R_0}} &= \alpha^{e}_{tu}(\mathbf{F},\mathbf{R_0}) - \alpha^{e}_{tu}(\mathbf{0},\mathbf{R_0}) \\ &= \sum_{v}\beta^{e}_{tuv}F_v + \frac{1}{2}\sum_{v,w}\gamma^{e}_{tuvw}F_vF_w + \cdots, \end{aligned} \tag{7}$$

$$\begin{aligned}\left(\Delta\alpha^{e}_{tu}\right)_{\mathbf{R_F}} &= \alpha^{e}_{tu}(\mathbf{F},\mathbf{R_F}) - \alpha^{e}_{tu}(\mathbf{0},\mathbf{R_0}) \\ &= \sum_{v}b^{\alpha}_{tuv}F_v + \frac{1}{2}\sum_{v,w}g^{\alpha}_{tuvw}F_vF_w + \cdots, \end{aligned} \tag{8}$$

as well as for β^{e}:

$$\left(\Delta\beta^{e}_{tuv}\right)_{\mathbf{R_0}} = \beta^{e}_{tuv}(\mathbf{F},\mathbf{R_0}) - \beta^{e}_{tuv}(\mathbf{0},\mathbf{R_0}) = \sum_{w}\gamma^{e}_{tuvw}F_w + \cdots, \tag{9}$$

$$\left(\Delta\beta^{e}_{tuv}\right)_{\mathbf{R_F}} = \beta^{e}_{tuv}(\mathbf{F},\mathbf{R_F}) - \beta^{e}_{tuv}(\mathbf{0},\mathbf{R_0}) = \sum_{w}g^{\beta}_{tuvw}F_w + \cdots, \tag{10}$$

where

$$b^{\alpha}_{tuv} = \beta^{e}_{tuv}(0;0,0) + \beta^{\mathrm{NR}}_{tuv}(-\omega;\omega,0)_{\omega\to\infty}, \tag{11}$$

$$g^{\alpha}_{tuvw} = \gamma^{e}_{tuvw}(0;0,0,0) + \gamma^{\mathrm{NR}}_{tuvw}(-\omega;\omega,0,0)_{\omega\to\infty}, \tag{12}$$

$$g^{\beta}_{tuvw} = \gamma^{e}_{tuvw}(0;0,0,0) + \gamma^{\mathrm{NR}}_{tuvw}(-2\omega;\omega,\omega,0)_{\omega\to\infty}. \tag{13}$$

The subscript $\omega\to\infty$ in Eqs. (11)–(13) refers to the infinite optical frequency approximation. Strictly speaking, it means that the ratios $(\omega_j/\omega)^2 = (\nu_j/\nu)^2$ are assumed to be negligible compared to unity. Again, the first-order anharmonic contributions (if nonzero) are fully accounted for. Finally, although not included above (or in this paper), the FF–NR method has recently been extended so as to yield the intensity-dependent refractive index, i.e. $\gamma^{\mathrm{NR}}(-\omega;\omega,-\omega,\omega)$, also known as the degenerate four-wave mixing coefficient.[54] The required electronic (hyper)polarizabilities at the field-dependent (and field-free) geometry are evaluated here by the CPKS method. CPKS values at the field-free geometry are compared with the finite-field calculations as a check on the latter.

III. RESULTS AND DISCUSSION

A. Band gap and orbital relaxation effect for (12,0) nanotube

As noted in the previous section, Table III shows the uncoupled sum-over-states (SOS) and CPHF and CPKS static electronic polarizabilities per BN unit obtained for the representative (12,0) nanotube using several different functionals. The SOS values vary from 5.505 Å^3 (LDA) to 1.927 Å^3 (HF) for $\alpha^{\parallel}$ (longitudinal component of the polarizability), and from 3.766 Å^3 (LDA) to 1.555 Å^3 (HF) for $\alpha^{\perp}$ (transverse component). They correlate strongly with the band gap, given in the same table. The parallel component, in particular, is almost directly proportional to the inverse band gap. Orbital relaxation, which is included in the CPHF and CPKS schemes, substantially weakens this relationship by dramatically reducing the differences between functionals, as documented previously in Ref. 36 for a given set of compounds. Here, for example, in the case of $\alpha^{\parallel}$, the HF value increases strongly from 1.927 to 3.322 Å^3, whereas the LDA value decreases by a small amount (5.505 to 5.313 Å^3). As a result, the LDA-HF ratio is reduced by about a factor of 1.7. With or without orbital relaxation, the Perdew-Burke-Ernzerhof (PBE) values are almost the same as LDA. Likewise, the two hybrid functionals yield similar results. Their behavior is intermediate between HF and the nonhybrid functionals, as might be expected. For $\alpha^{\perp}$, the situation is reversed from $\alpha^{\parallel}$. That is to say, when orbital relaxation is taken into account, the LDA value for the perpendicular component undergoes a large reduction (3.766 to 1.761 Å^3), whereas the HF value changes by only 10% (1.555 to 1.405 Å^3) and is reduced. The similarity between the two hybrid and the two nonhybrid functionals is preserved as is the intermediate behavior of the former.

The above data show that the uncoupled SOS scheme, although still in use,[18] can be a rather poor approximation depending upon the functional and the component of the polarizability. From here on, we shall solely use the the CPKS method with the B3LYP functional, which provides quite reasonable band gaps[55] and (hyper)polarizabilities for well-localized systems.[30,31] The calculated band gap in the (12,0)-SWBNNT considered here is about 5.9 eV (it ranges to 6.3 eV in the h-BN monolayer limit), in good agreement with the experimental values of 5.8–5.9 eV observed by Arenal *et al.*[8] for SWBNNTs and by Jaffrennou *et al.*[9,10] and Lee *et al.*[11,12] for multiwalled BNNT samples. Note that for B3LYP, it is important to take into account orbital relaxation as we have just seen.

B. Geometry optimization

The columns of Table IV labeled R_{B} and R_{N} give the optimized distance from the tube axis for the B and N atoms in the $(n,0)$ zigzag BNNTs, also known as *zigzag* BNNTs. These distances may be compared with the unrelaxed distance R_u. The latter is obtained by simply rolling up the BN monolayer, in which case both B and N atoms are at the same distance from the tube axis. For small values of n, $R_{\mathrm{N}} - R_{\mathrm{B}}$ can

TABLE IV. Calculated properties for the (n,0) series of BN nanotubes and the h-BN monolayer. δE and ΔE are defined in the text. Values reported are in μHa per BN unit (integers in parentheses indicate powers of 10). R_B and R_N are the distances (in Å) from the tube axis of the B and N atoms, respectively; R_u is the unrelaxed radius. BG is the band gap in eV. $\alpha^{\parallel}$ and $\alpha^{\perp}$ are the longitudinal and transverse components of the electronic and static polarizabilities per BN unit. The label ∞ indicates the asymptotic limit obtained by extrapolation as described in the text. The values in parentheses are estimated uncertainties on the last digit. The B3LYP hybrid density functional and 6-31G* basis set are used, with $S = 16$ ($S = 15$ for the layer) and $T_l = 8$. The row labeled Layer* gives the average of the monolayer parallel and perpendicular polarizabilities per BN unit, which should be equal to the large radius limit (∞ row) of the transverse nanotube polarizability.

							$\alpha^{\parallel}$		$\alpha^{\perp}$	
n	δE	ΔE	R_u	R_B	R_N	BG	α^e	α^0	α^e	α^0
3	−4.21(4)	6.94(4)	1.20	1.26	1.45	3.12	4.936	8.730	1.354	1.641
6	−4.12(3)	1.82(4)	2.40	2.41	2.51	4.39	4.764	7.770	1.453	1.713
9	−1.36(3)	8.12(3)	3.63	3.60	3.66	5.48	4.694	7.335	1.575	1.870
12	−6.99(2)	4.58(3)	4.79	4.80	4.84	5.94	4.644	7.293	1.680	2.024
16	−3.61(2)	2.64(3)	6.39	6.39	6.43	6.24	4.623	7.240	1.799	2.213
20	−2.21(2)	1.73(3)	7.98	7.99	8.02	6.36	4.613	7.201	1.895	2.373
24	−1.48(2)	1.23(3)	9.58	9.59	9.61	6.36	4.607	7.188	1.974	2.509
30	−9.06(1)	8.13(2)	11.98	11.99	12.00	6.35	4.603	7.179	2.068	2.679
36	−6.45(1)	5.77(2)	14.37	14.38	14.39	6.35	4.599	7.170	2.140	2.814
44	−4.17(1)	3.97(2)	17.57	17.57	17.58	6.35	4.597	7.160	2.214	2.959
50	−3.32(1)	3.11(2)	19.96	19.97	19.98	6.35	4.594	7.151	2.258	3.047
60	−2.34(1)	2.21(2)	23.96	23.96	23.97	6.35	4.594	7.152	2.317	3.167
∞	0	0				6.35	4.59(1)	7.11(3)	2.70(6)	4.00(3)
Layer*									2.703	4.001
Layer						6.34	4.591	7.111	0.815	0.890

be as large as 0.2 Å ($n = 3$), but falls rapidly to 0.1 Å at $n = 6$ and then to 0.04 Å at $n = 12$. Boron is always in the inner part of the tube and R_B differs the least from R_u. Figure 1 shows the convergence of the two nonequivalent B-N distances to the monolayer value as the size of the tube increases. ΔE in Table IV is the difference in energy per BN unit (in μHa) between the BNNT equilibrium structure and the equilibrium structure of the h-BN monolayer (monolayer more stable); the column labeled δE is the corresponding energy difference between the BNNT equilibrium structure and the value obtained by rigidly rolling up the equilibrium h-BN monolayer. In the following, if not differently stated, the nanotube radius will be considered as the average of the B and N cylinder radii.

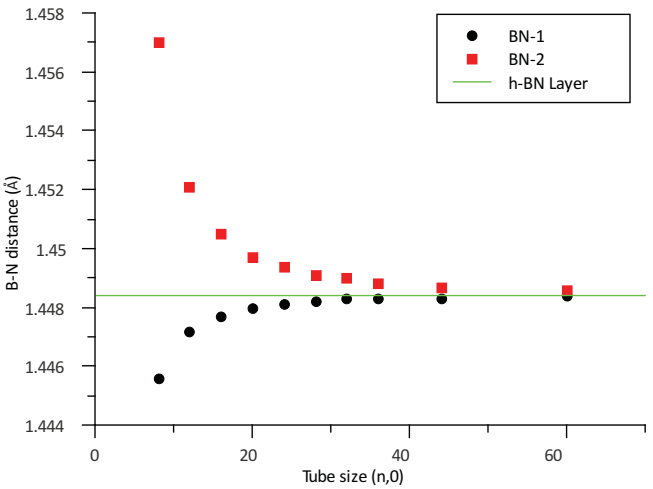

FIG. 1. (Color online) Behavior of the two nonequivalent BN distances as a function of n for (n,0) nanotubes. The horizontal line is the h-BN layer value.

C. Dependence of the static polarizability on tube radius

In Table IV, we also report the longitudinal and transverse components of the static electronic polarizability for the (n,0) nanotubes as a function of n. For the longitudinal ($\alpha^{\parallel}$) component, the static electronic and total [Eq. (1)] polarizabilities converge rapidly with n (or the nanotube radius R) to the corresponding monolayer values. Our extrapolations to $n \to \infty$ were done using a cubic (quadratic) polynomial in $1/n$ for the perpendicular (parallel) components of nanotubes with $n \geqslant 24$. We have extended previous calculations from radii smaller than 15 Å to radii as large as 24 Å so as to clearly exhibit the large R behavior. This is feasible with our approach since proper definition of the perturbative operator allows us to avoid the use of supercells, which are required with the use of a "sawtooth" potential as in previous work.[14,16] Nanotubes of 24-Å radius are comparable to those studied by Grujicica *et al.*[7] for their suitability as fluid-flow conduits in nanovalve applications.

As far as the transverse or perpendicular ($\alpha^{\perp}$) component is concerned, it has been noticed by Guo *et al.*[16] that there is a simple relation between the large radius limit of this component and the two different components of a single BN sheet. This can be justified by circular averaging or, as shown here, by the fact that the average polarizability is the same for both the sheet (monolayer) and the tube (and the same is true for the longitudinal component of both structures). If we consider the molar (per BN unit) perpendicular and parallel polarizabilities of the nanotube ($\alpha_n^{\perp}$ and $\alpha_n^{\parallel}$) and of the

monolayer ($\alpha_l^{\perp}$ and $\alpha_l^{\parallel}$), we can write, in the limit of infinite nanotube radius,

$$\begin{cases} 2\alpha_n^{\perp} + \alpha_n^{\parallel} = \alpha_l^{\perp} + 2\alpha_l^{\parallel}, \\ \alpha_n^{\parallel} = \alpha_l^{\parallel}, \end{cases} \tag{14}$$

which leads to

$$\alpha_n^{\perp} = \tfrac{1}{2}(\alpha_l^{\perp} + \alpha_l^{\parallel}). \tag{15}$$

For $\alpha_n^{\perp}$, our extrapolations of the CPKS static electronic and total value yield results that are in good agreement with Eq. (15) (see line Layer* in Table IV). The nanotube radii considered previously[14,16,17] were not sufficiently large to verify this relation with high accuracy as we have done here. Limiting the extrapolation to the set of BNNTs with $R < 15$ Å leads to about 5% error.

The behavior of the transverse static electronic polarizability as a function of nanotube radius has been the subject of much discussion[14,16,17,33] because of its bearing on models constructed to describe this property. Benedict *et al.*[33] proposed a conducting shell model for single-walled carbon nanotubes, which leads to a simple relationship between the unscreened and screened electronic polarizability per unit length [note that the polarizability is always given in this paper per BN unit except in Eqs. (16) and (17) below] or, equivalently, between α_{SOS} and α_{CPKS} (the superscript "e" is omitted for convenience):

$$\alpha_{\mathrm{CPKS}}^{\perp} = \frac{\alpha_{\mathrm{SOS}}^{\perp}}{1 + \frac{2\alpha_{\mathrm{SOS}}^{\perp}}{\tilde{R}^2}}. \tag{16}$$

Here, $\tilde{R} = R + \delta R$ is the effective radius. On this basis, Benedict *et al.* claim that, in the limit of large radius, $\alpha_{\mathrm{CPKS}}^{\perp}$ becomes proportional to R^2.

A more complicated relationship is obtained if the conducting shell is replaced by a dielectric shell with effective dielectric constant ϵ, which has been proposed as much more appropriate for the case of BNNTs. In that event, Lan *et al.*[17] obtain

$$\alpha^{\perp} = \frac{R_o^2\left(R_o^2 - R_i^2\right)(\epsilon^2 - 1)}{2\left[R_o^2(\epsilon+1)^2 - R_i^2(\epsilon-1)^2\right]}, \tag{17}$$

where $R_o = R + \delta R/2$ and $R_i = R - \delta R/2$. It is easy to show that this equation predicts a linear dependence on the radius in the large-R limit.

A plot of our $\alpha_{\mathrm{B3LYP}}^{\perp}$ (per unit length) versus R is shown in Fig. 2 (the equilibrium lattice parameter is almost independent of the nanotube size, varying from 4.345 to 4.337 Å for $12 \leqslant n \leqslant 60$). The linear R dependence predicted by the model of Lan *et al.* is clearly confirmed for $R \gtrsim 12$ Å. We then fit the entire curve to Eq. (17) to obtain an effective dielectric constant of $\epsilon = 6.19$ and a shell thickness $\delta R = 2.08$ Å. Our value for ϵ is reasonably close to the GGA (PBE) result ($\epsilon = 5.90$) of Lan *et al.,* but substantially smaller than their shell thickness ($\delta R = 2.50$ Å). The difference in the fitting parameters arises from the difference in the functionals. In order to see that is the case, Lan's curve is also shown in Fig. 2, along with (CPKS) results that we have obtained using the PBE functional instead of B3LYP. Clearly, our PBE curve is almost indistinguishable from that of Lan. As a final remark, we also note that, for small R, the nonlinear dependence upon the radius is also well duplicated by Eq. (17).

D. FF–NR vibrational (hyper)polarizabilities

The FF–NR method was employed to evaluate the nuclear-relaxation approximation for the so-called ionic (= vibrational) contribution to the transverse static and dynamic (hyper)polarizabilities of representative (6,0), (9,0), and (12,0) BN nanotubes. Calculations for larger nanotubes, as well as their analysis, is beyond the scope of this paper and will be presented elsewhere. We have, however, chosen to examine the smaller nanotubes here in order to demonstrate the viability of the FF–NR method for application to materials of this type, which does not seem to have been previously recognized. The results obtained also serve to indicate the variety and potential significance of the vibrational properties that are accessed.

In our calculations, a static field perpendicular to the nanotubes was applied and a full geometry optimization was performed for each nanotube, starting from the zero-field equilibrium geometry $\mathbf{R_0}$. Then, the electronic dipole moment μ, CPKS polarizability α, and CPKS first hyperpolarizability β were calculated,[38] as a function of field, for both the field-free geometry $\mathbf{R_0}$ and the optimized field-dependent geometry $\mathbf{R_F}$. A fitting of the CPKS properties gives the vibrational (nuclear-relaxation) contributions to static and dynamic (hyper)polarizabilities according to Eqs. (4)–(6) and (11)–(13). Six different field values were considered in the interval 5×10^{-4}–1×10^{-2} a.u. The fitting procedures that were used are described below. From now on, the Cartesian indices $tuvw$ of Eqs. (4)–(6) and (11)–(13) are omitted since all (hyper)polarizabilities refer to the diagonal element of the tensor along the field direction z. Equation (3) yields the static nuclear-relaxation (hyper)polarizabilities. Because the field-free nanotube has a center of inversion, the first hyperpolarizability (b^{μ}) vanishes. Thus, a plot [see Fig. 3 for the (12,0) nanotube] of $[\mu(\mathbf{F},\mathbf{R_F}) - \mu(\mathbf{0},\mathbf{R_0})]/F$ versus field yields a^{μ} as the intercept and g^{μ} as the coefficient of the quadratic term (the linear term vanishes). For an initial test,

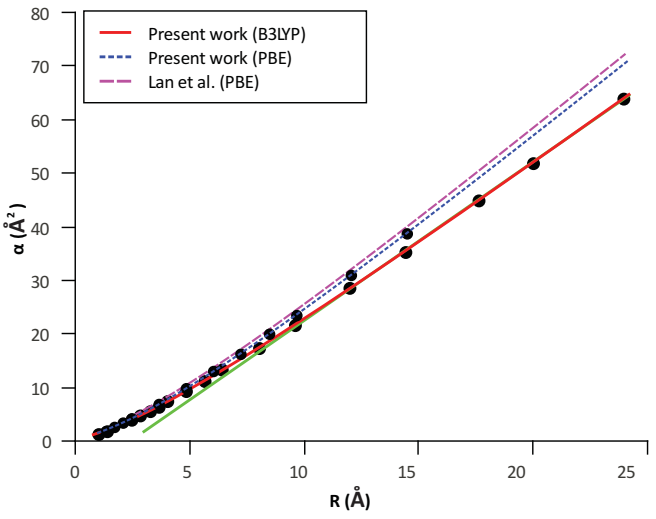

FIG. 2. (Color online) Transverse polarizability per unit length of BN nanotubes as a function of tube radius.

TABLE V. Electronic and vibrational contributions to the transverse (hyper)polarizabilities for the (6,0), (9,0), and (12,0) nanotubes obtained by the FF–NR method using Eqs. (2)–(13) as described in the text (see equations for definition of symbols). The static electronic contribution to the second hyperpolarizability obtained analytically with the CPKS method ($\gamma^e_{\rm CPKS}$) is also reported for comparison. Polarizabilities in Å^3; hyperpolarizabilities in a.u.

n	6	9	12
$\alpha^e_{\rm FF}(0;0)$	1.454	1.576	1.679
a^μ	1.713	1.870	2.024
$\gamma^e_{\rm CPKS}(0;0,0,0)$	632.3	929.6	1337
$\gamma^e_{\rm FF}(0;0,0,0)$	635.5	929.1	1361
g^μ	1785	4433	9498
g^α	772.6	1645	3199
g^β	460.8	722.6	1043
$\gamma^{\rm NR}(0;0,0,0)$	1152	3503	8161
$\gamma^{\rm NR}(-\omega;\omega,0,0)_{\omega\to\infty}$	140.3	715.4	1862
$\gamma^{\rm NR}(-2\omega;\omega,\omega,0)_{\omega\to\infty}$	−171.5	−207.0	−294.0

we replaced $\mu(\mathbf{F},\mathbf{R_F})$ by $\mu(\mathbf{F},\mathbf{R_0})$, as in Eq. (2), and verified that the finite-field electronic (hyper)polarizabilities agreed well with the CPKS values. The finite-field results for α^e shown in Table V are exactly the same (to the number of significant figures given) as the CPKS values reported in Table IV, whereas for γ^e, the two differ at most by 1.8%, i.e., $\gamma^e_{\rm FF} = 1361$ versus $\gamma^e_{\rm CPKS} = 1337$ a.u. in the case of the (12,0) nanotube. As shown below, the vibrational contributions to the static γ are much larger than this uncertainty.

The values for a^μ determined from fitting our computed data to Eq. (3) [cf. Fig. 3(a) for the (12,0) nanotube] can be compared with α^0 in Table IV. Since both quantities correspond to the double harmonic approximation, the excellent agreement obtained provides a check of both methods of calculation. From Eq. (6), we obtain the vibrational (nuclear relaxation) $\gamma^{\rm NR}(0;0,0,0)$. It is noteworthy that this quantity is substantially larger than the static pure electronic γ^e (see Table V) and grows much more rapidly with n over the range ($n = 6$–12) considered here. In particular, $\gamma^{\rm NR}$ is roughly twice as large as γ^e for $n = 6$, whereas the same ratio is more than 6 for $n = 12$.

A plot of $[\alpha^e(\mathbf{F},\mathbf{R_F}) - \alpha^e(\mathbf{0},\mathbf{R_0})]$ versus field is shown in Fig. 3(b) for $n = 12$. In this case, the linear term again vanishes due to symmetry and one obtains a pure quadratic function (with zero intercept), which yields g^α and $\gamma^{\rm NR}(-\omega;\omega,0,0)_{\omega\to\infty}$ according to Eq. (12). Table V shows that the relative importance of the latter, i.e., the vibrational dc-Kerr effect term, also increases with n faster than the static electronic γ^e. At $n = 12$, this vibrational term is the larger of the two by a factor of about 1.40 and continuing to grow more so with increasing n. As expected, the magnitude of the nuclear-relaxation contribution to the dc-Kerr effect, although quite substantial, is less important than the corresponding contribution to the static vibrational γ. This is due to the fact that the number of static fields that describe the nonlinear process is reduced from three (static) to two (dc-Kerr).[56]

Finally, Fig. 3(c) shows a plot of $[\beta(\mathbf{F},\mathbf{R_F}) - \beta(\mathbf{0},\mathbf{R_0})]$ versus field, again, for the (12,0) nanotube. This curve is

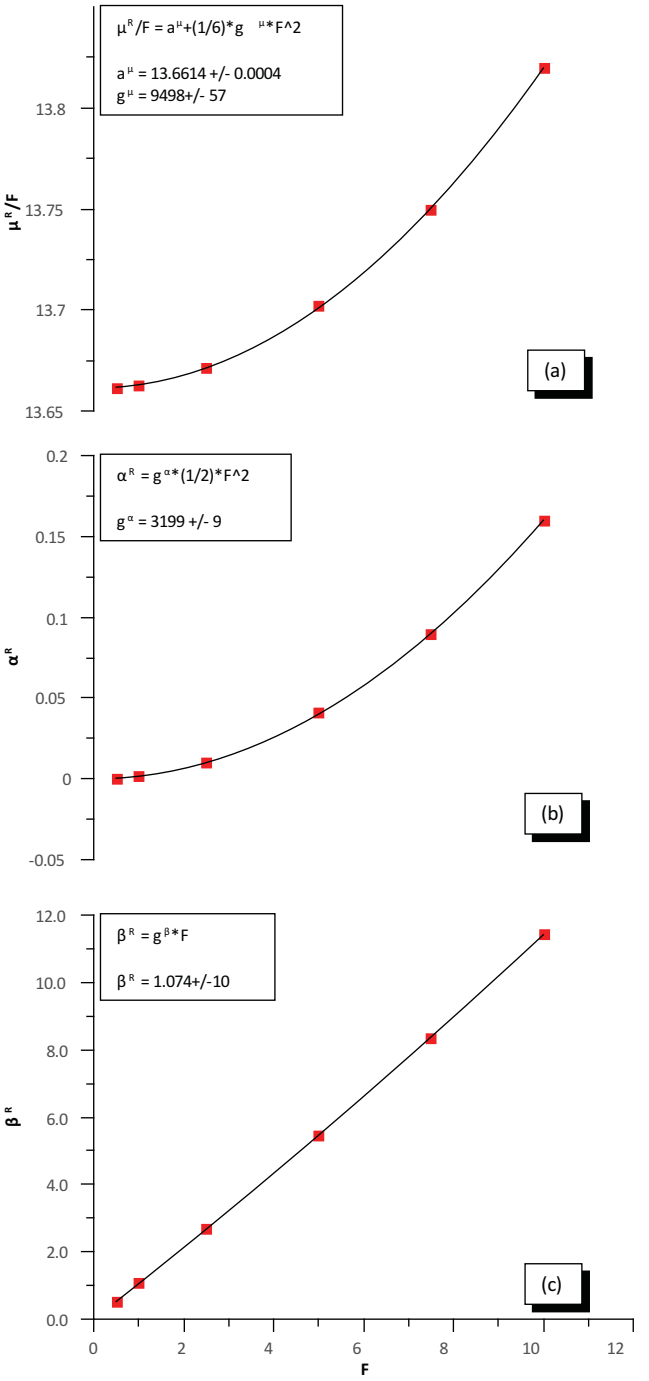

FIG. 3. (Color online) Dependence of the $\frac{\mu^R}{F} = \frac{(\Delta\mu_z)_{\mathbf{R_F}}}{F}$, $\alpha^R = (\Delta\alpha^e_{zz})_{\mathbf{R_F}}$, and $\beta^R = (\Delta\beta^e_{zzz})_{\mathbf{R_F}}$ functions for the (12,0) zigzag nanotube, as defined in Eqs. (2), (8), and (10), on the applied electric-field F value (in 10^{-3} a.u.). The fitting parameters are given in the inset of each figure.

linear with zero intercept. From the slope, we find $g^\beta = \gamma^e(0;0,0,0) + \gamma^{\rm NR}(-2\omega;\omega,\omega,0)_{\omega\to\infty} = 1074$ a.u., which, after subtracting the static electronic γ^e, yields the nuclear-relaxation contribution to dc second-harmonic generation. Our results for the latter property are also reported in Table V, where it is seen to be significant but further reduced (in

comparison with the nuclear-relaxation dc-Kerr value) since a single static field describes this process. It is, furthermore, not growing faster than the static electronic γ^e.

IV. CONCLUSIONS AND FUTURE WORK

In this paper, we have studied the electronic and nuclear electric-field response of BN nanotubes at the CPKS B3LYP/6-31G* level of treatment using the CRYSTAL code. For the longitudinal and transverse linear response (polarizability $= \alpha$), a set of $(n,0)$ zigzag nanotubes ranging from $n = 3$ to 60 were considered; for the transverse nonlinear response (second hyperpolarizability $= \gamma$), which has not previously been investigated, a few representative tubes within the range $n = 6$–12 were examined.

It was established that the orbital relaxation included in the CPKS method, but not in a sum-over-states calculation, makes an important contribution to the electronic α^e, which depends upon the particular component (parallel or perpendicular). The effect of orbital relaxation depends upon the particular component (parallel or perpendicular) and one may anticipate that it will be even more important for γ. In the case of α^e, the B3LYP CPKS values are substantially different from those obtained with nonhybrid functionals (LDA, PBE) and intermediate between the latter and Hartree-Fock.

From the results for large radius nanotubes (much larger than previously studied), we were able to make an accurate comparison, in the limit $n \to \infty$, between the nanotube and a planar sheet. Thus, it was verified that the geometries are the same and that the transverse static α of the nanotube is equal to the average of the parallel and perpendicular components of the sheet. This result was found for both the electronic and vibrational contributions. In addition, we confirmed that α^e per unit length depends linearly on the tube radius for large n, as predicted by Lan *et al.* based on a dielectric shell model of the BN nanotube. On the other hand, our calculated shell thickness is substantially smaller than theirs due to the use of different basis sets: Gaussian-type atomic orbitals here versus plane waves with pseudoptential in the paper of Lan *et al.*

The nuclear (i.e., vibrational or "ionic") electric-field response was determined by two different methods: (i) from Born effective charges and vibrational frequencies; and (ii) by the finite-field–nuclear-relaxation (FF–NR) technique. The latter is applied here for the first time to a nanotube or any other periodic material. In principle, both approaches should yield identical results for the static α, although the FF–NR method avoids calculation of the dynamical matrix. For the representative (6,0), (9,0), and (12,0) nanotubes, we confirmed that the same (transverse) static vibrational α is obtained in practice as well. By using the FF–NR method, we were also able to obtain static and dynamic (infinite optical frequency approximation) vibrational hyperpolarizabilities. These hyperpolarizabilities include all first-order corrections for mechanical and electrical anharmonicity (as well as a second-order correction for the static γ). Our results highlight the significance of the nuclear response, which increases in importance with the radius of the nanotube. In particular, for the (12,0) nanotube, the vibrational contribution to the transverse static γ is more than 6 times larger than the corresponding static γ^e; for the dc-Kerr effect, it is about 1.4 times larger.

There are, clearly, a number of issues that deserve further attention. These include the behavior of the electronic hyperpolarizability, as well as the relative importance of the nuclear response, as a function of tube radius. In both cases, only a few representative small nanotubes and only the transverse component were considered. An implementation for the longitudinal electronic response is already present in the CRYSTAL code. That is not true for the FF–NR treatment of the vibrational response. However, the methodology needed for periodic directions is available, at least for quasi-1D systems,[29,57] and implementation is in progress.

ACKNOWLEDGMENTS

The authors thank CINECA for granting access to supercomputing resources (ISCRA Award No. HP10AC4ZGA.2010).

[1] S. Ijima, Nature (London) **354**, 96 (1991).
[2] M. U. Kahaly and U. V. Waghmare, J. Nanosci. Nanotechnol. **7**, 1787 (2007).
[3] A. Rubio, J. L. Corkill, and M. L. Cohen, Phys. Rev. B **49**, 5081 (1994).
[4] X. Blase, A. Rubio, S. Louie, and M. Cohen, Europhys. Lett. **28**, 335 (1994).
[5] N. Chopra, R. Luyken, V. Crespi, M. Cohen, S. Louie and A. Zettl, Science **269**, 966 (1995).
[6] S. J. C. Y. Chen, J. Zou and G. L. Caer, Appl. Phys. Lett. **84**, 2430 (2004).
[7] M. Grujicica, G. Cao, and W. N. Roy, Appl. Surf. Sci. **246**, 149 (2005).
[8] R. Arenal, O. Stéphan, M. Kociak, D. Taverna, A. Loiseau, and C. Colliex, Phys. Rev. Lett. **95**, 127601 (2005).
[9] P. Jaffrennou, F. Donatini, J. Barjon, J. S. Lauret, A. Maguer, B. Attal-Trétout, F. Ducastelle, and A. Loiseau, Chem. Phys. Lett. **442**, 372 (2007).
[10] P. Jaffrennou, J. Barjon, J. S. Lauret, A. Maguer, D. Golberg, B. Attal-Trétout, F. Ducastelle, and A. Loiseau, Phys. Status Solidi B **244**, 4147 (2007).
[11] C. H. Lee, J. Wang, V. K. Kayashta, J. Y. Huang, and Y. K. Yap, Nanotechnology **19**, 455605 (2008).
[12] C. H. Lee, M. Xie, V. Kayashta, J. Wang, and Y. K. Yap, Chem. Mater. **22**, 1782 (2010).
[13] C. Sun, H. Yu, L. Xu, Q. Ma, and Y. Qian, J. Nanomater. **2010**, 163561 (2010).
[14] G. Y. Guo and J. C. Lin, Phys. Rev. B **71**, 165402 (2005).
[15] S. Hao, G. Zhou, W. Duan, J. Wu, and B. L. Gu, J. Am. Chem. Soc. **128**, 8453 (2006).

[16]G. Y. Guo, S. Ishibashi, T. Tamura, and K. Terakura, Phys. Rev. B **75**, 245403 (2007).
[17]H.-P. Lan, L.-H. Ye, S. Zhang, and L.-M. Peng, Appl. Phys. Lett. **94**, 183110 (2009).
[18]V. A. Margulis, E. E. Muryumin, and E. A. Gaiduk, Phys. Rev. B **82**, 235426 (2010).
[19]H. Dai, Acc. Chem. Res. **35**, 1035 (2002).
[20]C. T. White, D. H. Robertson, and J. W. Mintmire, Phys. Rev. B **47**, 5485 (1993).
[21]L. Wang, J. Lu, L. Lai, W. Song, M. Ni, Z. Gao, and W. N. Mei, J. Phys. Chem. C **111**, 3285 (2007).
[22]B. Champagne, E. A. Perpète, S. J. A. van Gisbergen, E. J. Baerends, J. G. Snijders, C. Soubra-Ghaoui, K. Robins, and B. Kirtman, J. Chem. Phys. **109**, 10489 (1998).
[23]B. Champagne, E. A. Perpète, S. J. A. van Gisbergen, E. J. Baerends, J. G. Snijders, C. Soubra-Ghaoui, K. Robins, and B. Kirtman, J. Chem. Phys. **110**, 11664 (1999).
[24]S. J. A. van Gisbergen, P. R. T. Schipper, O. V. Gritsenko, E. J. Baerends, J. G. Snijders, B. Champagne, and B. Kirtman, Phys. Rev. Lett. **83**, 694 (1999).
[25]O. Loboda, R. Zalesny, A. Avramopoulos, J. M. Luis, B. Kirtman, N. Tagmatarchis, H. Reis, and M. G. Papadopoulos, J. Phys. Chem. A **113**, 1159 (2008).
[26]S. Kümmel, L. Kronik, and J. P. Perdew, Phys. Rev. Lett. **93**, 213002 (2004).
[27]D. M. Bishop, M. Hasan, and B. Kirtman, J. Chem. Phys. **103**, 4157 (1995).
[28]B. Kirtman, J. M. Luis, and D. M. Bishop, J. Chem. Phys. **108**, 10008 (1998).
[29]M. Springborg and B. Kirtman, Phys. Rev. B **77**, 045102 (2008).
[30]R. Orlando, V. Lacivita, R. Bast, and K. Ruud, J. Chem. Phys. **132**, 244106 (2010).
[31]M. Ferrero, B. Civalleri, M. Rérat, R. Orlando, and R. Dovesi, J. Chem. Phys. **131**, 214704 (2009).
[32]V. Lacivita, M. Rérat, B. Kirtman, M. Ferrero, R. Orlando, and R. Dovesi, J. Chem. Phys. **131**, 204509 (2009).
[33]L. X. Benedict, S. G. Louie, and M. L. Cohen, Phys. Rev. B **52**, 8541 (1995).
[34]L. Wirtz, M. Lazzeri, F. Mauri, and A. Rubio, Phys. Rev. B **71**, 241402 (2005).
[35]M. Ferrero, M. Rérat, R. Orlando, and R. Dovesi, J. Comput. Chem. **29**, 1450 (2008).
[36]M. Rérat, M. Ferrero, E. Amzallag, I. Baraille, and R. Dovesi, J. Phys.: Conf. Ser. **117**, 12023 (2008).
[37]M. Ferrero, M. Rérat, B. Kirtman, and R. Dovesi, J. Chem. Phys. **129**, 244110 (2008).
[38]R. Orlando, R. Bast, K. Ruud, B. Kirtman, and R. Dovesi (unpublished).
[39]R. Dovesi, R. Orlando, B. Civalleri, C. Roetti, V. R. Saunders, and C. M. Zicovich-Wilson, Z. Kristallogr. **220**, 571 (2005).
[40]R. Dovesi, V. R. Saunders, C. Roetti, R. Orlando, C. M. Zicovich-Wilson, F. Pascale, B. Civalleri, K. Doll, N. M. Harrison, I. J. Bush, P. D'Arco, and M. Llunell, *CRYSTAL 2009 User's Manual* (University of Torino, Torino, 2009).
[41]F. Pascale, C. M. Zicovich-Wilson, R. Orlando, C. Roetti, P. Ugliengo, and R. Dovesi, J. Phys. Chem. B **109**, 6146 (2005).
[42]M. Prencipe, F. Pascale, C. Zicovich-Wilson, V. Saunders, R. Orlando, and R. Dovesi, Phys. Chem. Miner. **31**, 559 (2004).
[43]S. Tosoni, F. Pascale, P. Ugliengo, R. Orlando, V. R. Saunders, and R. Dovesi, Mol. Phys. **103**, 2549 (2005).
[44]K. Doll, Comput. Phys. Commun. **137**, 74 (2001).
[45]K. Doll, N. M. Harrison, and V. R. Saunders, Int. J. Quantum Chem. **82**, 1 (2001).
[46]B. Civalleri, P. D'Arco, R. Orlando, V. R. Saunders, and R. Dovesi, Chem. Phys. Lett. **348**, 131 (2001).
[47]C. G. Broyden, J. Inst. Math. Appl. **6**, 76 (1970).
[48]R. Fletcher, Comput. J. **13**, 317 (1970).
[49]D. Goldfarb, Math. Comput. **24**, 23 (1970).
[50]D. F. Shanno, Math. Comput. **24**, 647 (1970).
[51]R. Resta, Rev. Mod. Phys. **66**, 809 (1994).
[52]R. D. King-Smith and D. Vanderbilt, Phys. Rev. B **49**, 5828 (1994).
[53]B. Kirtman and D. M. Bishop, Chem. Phys. Lett. **175**, 601 (1990).
[54]B. Kirtman and J. M. Luis, J. Chem. Phys. **128**, 114101 (2008).
[55]J. Muscat, A. Wander, and N. Harrison, Chem. Phys. Lett. **342**, 397 (2001).
[56]B. Kirtman (unpublished).
[57]M. Springborg and B. Kirtman, J. Chem. Phys. **126**, 104107 (2007).